Biointerface Research in Applied Chemistry
Open-Access Journal (ISSN: 2069-5837)

Article
Volume 14, Issue 1, 2024, 21
https://doi.org/10.33263/BRIAC141.021

Improvement of Permittivity, Electric Modulus, and Permeability of BariumNanoparticles Ferrite with Nonmagnetic ions (Zn^{+2})

Sadiq H. Khoreem [1,2,3,*], A. H. AL-Hammadi [3]

[1] Physics Department, Faculty of Science, Sa'ada University, Sa'ada, Yemen
[2] Dept. of Optometry and Vision Science, Faculty of Medical Sciences, Al-Razi University, Sana'a, Yemen
[3] Physics Department, Faculty of Science, Sana'a University, Sana'a, Yemen
* Correspondence: khoreems@yahoo.com (S.H.K.);

Scopus Author ID 57571836200
Received: 7.01.2023; Accepted: 22.02.2023; Published: 3.02.2023

Abstract: The effects of composition, temperature, and frequency-dependent dielectrics Properties of barium-nickel-based ferrites have been investigated. The conventional ceramic technique prepared the compositions $BaNi_{2-x}Zn_xFe_{16}O_{27}$ (x = 0.0, 0.4, 1.2, and 2). The relatively high values of the dielectric constant at low frequencies are due to the interfacial polarization, which ensures that the samples can be fairly considered to be formed of well-conducting grains and poorly-conducting grain boundaries according to Koop's model. Dielectric results showed that zinc concentration at the composition x = 0.4 is sufficient to reduce the dielectric constant and loss tangent at low frequencies. Overall, the dielectric properties of this sample made them a suitable candidate for flexible supercapacitors and are best suited for high-frequency region applications. The existence of gradually shifted shoulders in the tan vs. temperature curves towards higher frequencies ensures the presence of two types of charge carriers. The results indicate that the initial permeability of the synthesized sample ferrites increases with increasing zinc ion concentration. The initial magnetic permeability decreases as Zn^{2+} ion substitution increases. The substitution of Zn ions greatly enhanced the dielectric constant, dielectric loss, as well as initial permeability.

Keywords: W-type barium ferrites; permittivity; initial permeability; electric modulus; nonmagnetic ions.

1. Introduction

Nanoparticles have different electrical, optical, microstructural, and magnetic characteristics, which are different from the corresponding stable-state bulk properties. This is because of the small size effect, dimensions, surface influence, or quantum impact [1, 2]. Metallic nanoparticles have been comprehensively examined due to their practical significance and technical importance for wide-range applications in industry, electronic devices, magnetic materials, etc. [3, 4]. Ferrites are divided into different categories depending on their crystal structure: spinel ferrite, garnet, and hexagonal ferrites, all of which have their importance [5]. Substituted W-type ferrite has promising potential candidates for technological use because of its intriguing features. These hexagonal ferrites have a ferromagnetic nature at both operating and ambient temperatures. More than 90% of permanent magnets are produced worldwide based on this compound. So, this compound was a deep semiconductor with a ferrimagnetic

structure at room temperature [6–8]. Furthermore, a large spontaneous polarization and multi-ferric properties at room temperature recently discovered in barium hexaferrite were substituted by diamagnetic cations [9]. Various ferrite groups, such as manganese-zinc, nickel-zinc, and magnesium-manganese, are vital for high-tech applications [10–12]. Only nickel-zinc bulk ferrite nanoparticles are promising and suitable for use in high-frequency applications [10, 13–14]. Eddy currents at high frequencies are a major drawback; they restrict the operation at higher frequencies. This problem can be overcome by increasing the material's electrical resistance and achieving a higher magnetic moment. The electrical resistance can be directly increased by removing the cross-functional and cross-domain wall and converting the material into fine particulate matter. [15, 16]. As grain size increases, grain boundaries form and obstruct electron passage, reducing eddy current losses [17–20]. In addition, doping BaNi ferrite with Zn ions has attracted significant attention due to ferrites' interesting and enhanced properties. Here, we explain the effects of nonmagnetic ions dopant (Zn ions) on barium-nickel nanoferrites. In the present study, the dielectric properties of $BaNi_{2-x}Zn_xFe_{16}O_{27}$ (x = 0, 0.4, 1.2, 2) ferrites were examined as a function of frequency, temperature, and composition, with variation concentration from Zn^{+2} ions doping.

2. Materials and Methods

A composition of samples of the $BaNi_{2-x}Zn_xFe_{16}O_{27}$ w-type hexaferrite (with x = 0.0, 0.4, 1.2, and 2) has been prepared using the usual ceramics technique as mentioned earlier [21,22], and shown in Figure 1. The sample powder was pressed under a pressure of 4 tons per square centimeter at room temperature to form discs and toroids. This disc and toroid were sintered at 1250 K for 4 hours and slowly cooled to room temperature by turning the furnace. After that, the discs were polished to obtain two smooth, uniform parallel plate surfaces, and the surfaces were coated with a thin layer of silver as a good contacting material for measurements of the AC conductivity and dielectric properties. The dielectric was measured under vacuum at different temperatures and frequencies using the complex impedance measuring technique (Lock-in amplifier Stanford SR 510 type, USA).

3. Results and Discussion

The property of a dielectric that determines the electrostatic energy stored per unit volume for unit potential gradient indicates the degree to which a medium can resist the flow of charge. It describes a material's ability to store charge when used as a capacitor's dielectric.

3.1. Real part of permittivity dependence on composition.

The dielectric constant (έ) in the ferrites was affected by a number of factors, such as the preparation methods' structure, dopants, and microstructure. The dielectric constant ε' as a function of composition for all samples at selected frequencies is shown in Figure 2 (a, and b). It has been observed that in Figure 2, the dielectric constant increases with the increase in Zn concentration. The decrease in the dielectric constant values might occur due to the increasing grain size values. With increasing zinc concentration, the grain size increases, and the conversion of Fe^{3+} into Fe^{2+} ions increases. Zinc ions occupy tetrahedral (A) sites, whereas Ni ions prefer to go to octahedral (B) sites [22].

Figure 1. Flow chart of rare-earth ferrite sample preparation technique by the usual ceramic method.

Also, with increasing Zn ions, the Fe ions migration from the octahedral site to the tetrahedral site causes a decrease in the hopping between Fe^{3+} and Fe^{2+}, leading to the real part of permittivity decreased [23]. When Zn is added in place of Ni^{2+} ions, some Fe^{3+} ions are converted to Fe^{2+} ions to maintain charge neutrality. As a result, hopping between Fe^{3+} and Fe^{2+} ions increases, and the resistance of grains decreases. The probability of this increases electrons reaching the grain boundary. Consequently, polarization and the dielectric constant both increase [21]. The dielectric polarization mechanism in ferrites is similar to the conduction mechanism [24], where poorly conducting grain boundaries play a main role at lower frequencies, thereby ε′ showing higher values at lower frequencies.

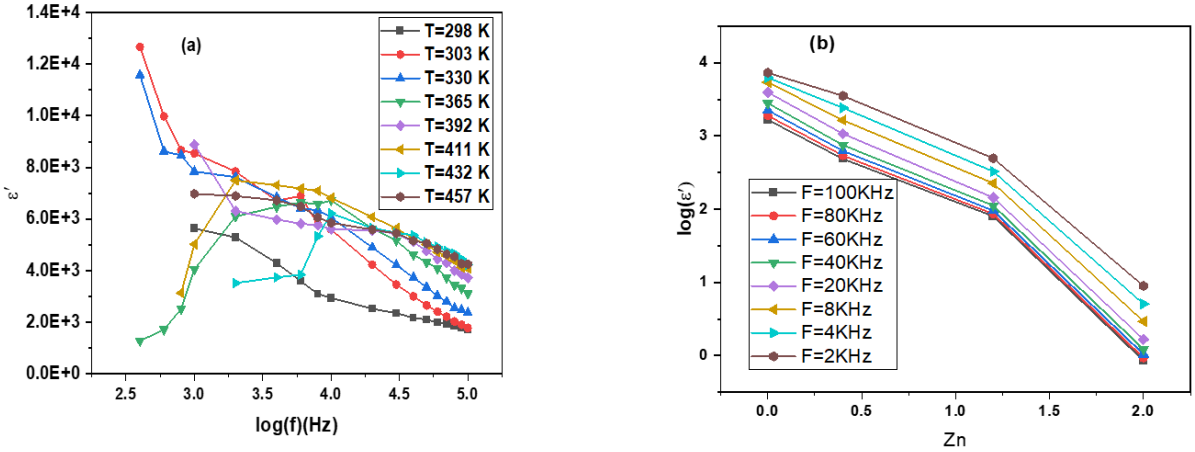

Figure 2. (a) Relationship real part of dielectric constant with log frequency at different temperatures; (b) Relationship between zinc concentration and the real part of permittivity of $BaNi_{2-x}Zn_xFe_{16}O_{27}$ (x=0.0, 0.4, 1.2, and 2) at different frequencies at room temperature.

Furthermore, at higher frequencies, conducting grains are activated. In the low-frequency region, the doping of Zn causes low values of dielectric properties compared to x =

0.0 (pure barium ferrite), as shown in Figure 2.a. This could be related to the increase in grain size with Zn ion substitution. The grain size increase reduced grain boundaries, thereby decreasing the possibility of electron hopping. This causes the decrease in the dielectric constant of Zn substituted BaW hexaferrite, as shown in Figure 2. b).

3.2. Real part of permittivity dependence on temperature.

The real part of permittivity (έ) for Zn-substituted Ba-Ni ferrites was calculated using the flowing equation (1):

$$\varepsilon' = \frac{C}{C_\circ} = \frac{11.3\ d}{A} C = \frac{11.3\ d}{A} \frac{I}{\omega} \sin \emptyset \quad (1)$$

where C is the disc capacitance, d thickness, and A area.

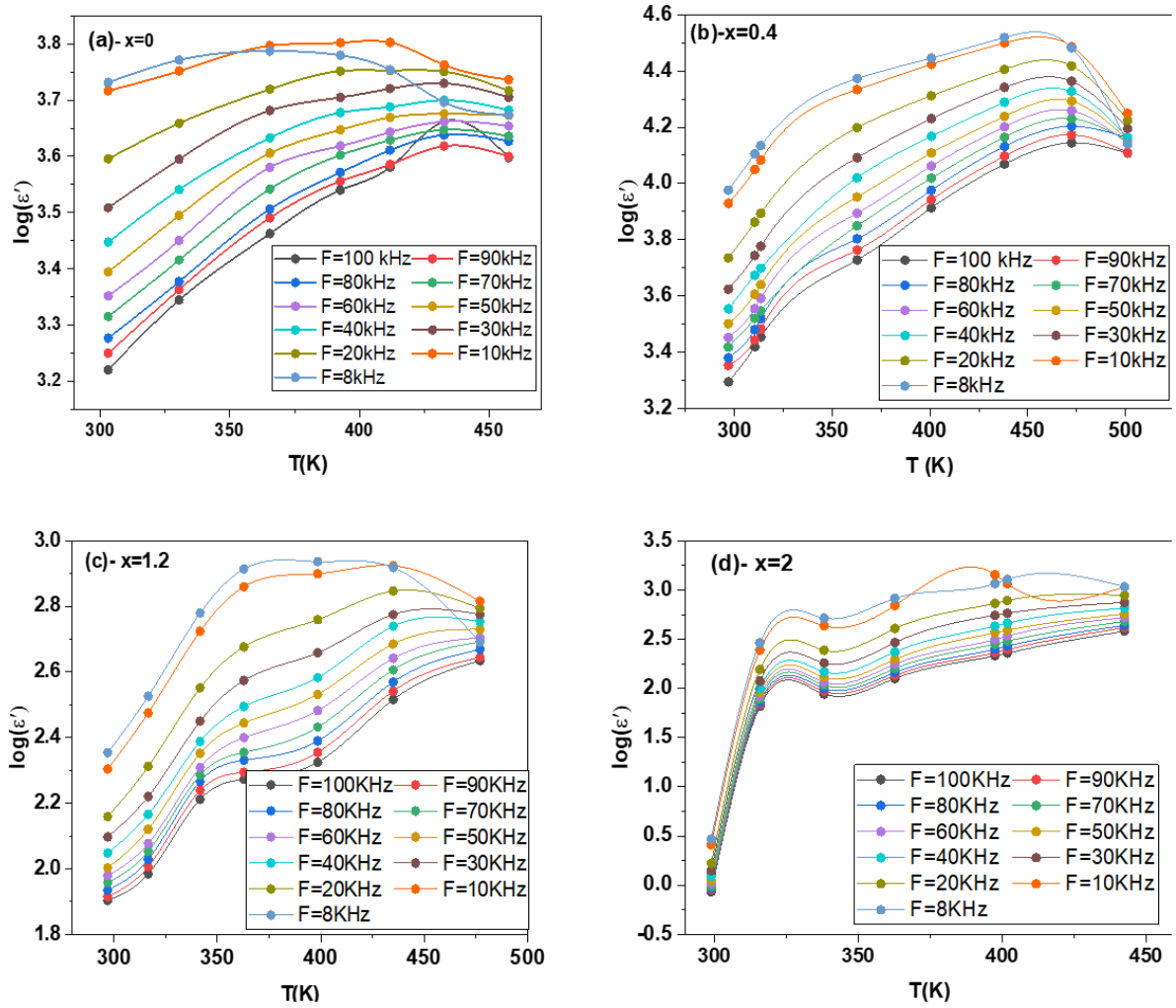

Figure 3. Temperature dependence of dielectric constant (ε') of $BaNi_{2-x}Zn_xFe_{16}O_{27}$ (a) x= 0.0; (b) x= 0.4;(c) at x = 1.2; and (d) at x = 2, at different frequencies.

Figure 3 shows that the dielectric constant increases with temperature at all frequencies. At lower frequencies, the increase in dielectric constant is very large with the increase in temperature, while at higher frequencies, this increase is very small. The dielectric constant of a material depends upon four kinds of polarization: dipolar, interfacial, electronic, and ionic. Dipolar and interfacial polarizations are important at lower frequencies [25]. Both polarizations depend on the temperature variation. The surface polarization will increase with the temperature rise. This increase in polarization is due to the creation of crystal defects. The dipolar polarization decreases with the rise in temperature. The rapid increase in dielectric

constant with the rise in temperature at lower frequencies shows that the effect of temperature is more pronounced on the interfacial than on the dipolar polarization. Electronic and ionic polarizations are the main partners at higher frequencies, and their temperature dependence is important. A constant and low value of the dielectric constant at higher frequencies is understandable.

3.3. Frequency dependence of dielectric constant.

The real part of permittivity for the zinc-doped barium ferrite sample is shown in Figure 4; with increasing frequency, the real part of permittivity decreased. This means that the real part of permittivity decreases at high frequencies and low temperatures, and dispersion is also observed, while at higher frequencies, it is frequency-independent. The real part of permittivity behaviors follows the Maxwell-Wagner model [26, 27]. The dielectric material's inhomogeneous structure is the main reason for the space charge polarization according to the presence of higher conductivity phases (grains) inside the insulating matrix (grain boundaries). An externally provided AC electric field causes a localized charge accumulation at the grain boundary [28]. The polarization results from the accumulation of electrons at the grain borders When the resistivity of the grain boundary is sufficiently high. It takes a finite amount of time for space charge carriers to build up in a dielectric to align their axes parallel to an alternating electric field. When the frequency of field reversal increases, fewer charge carriers can cross the grain boundary. As a result, they are unable to keep up with the field, and their directional alternation is delayed [28].

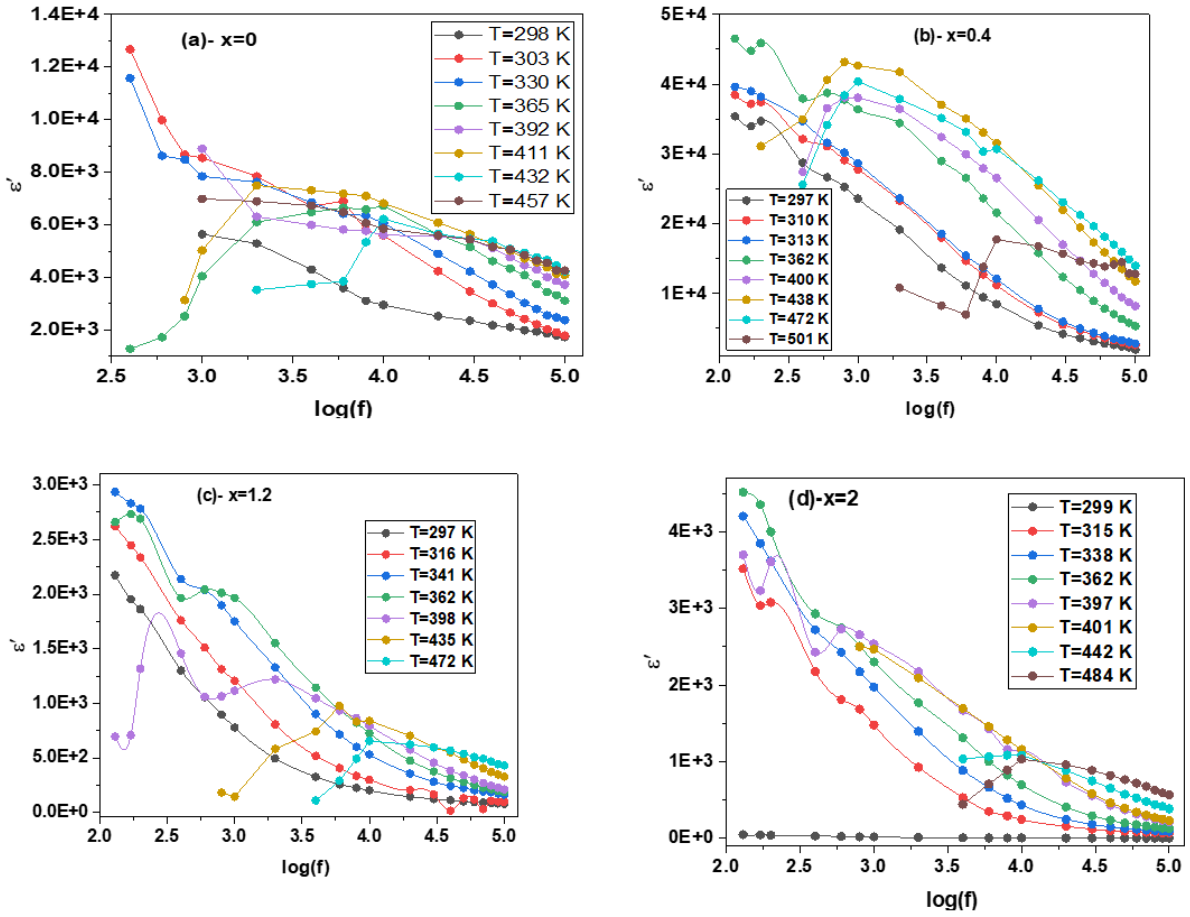

Figure 4. Dielectric constant dependence of frequency (ε′) of $BaNi_{2-x}Zn_xFe_{16}O_{27}$,(a) x= 0.0, (b) x= 0.4,(c) at x = 1.2, and (d) at x = 2), at different temperatures.

So, the reduction in polarization at grain boundaries caused the decrease in charge carriers, and the dielectric constant decreased. According to the authors [29], polarization in ferrites is a conduction-like phenomenon. The local displacement of electrons in the direction of the applied field as a result of the electron exchange between Fe^{2+} and Fe^{3+} establishes polarization. The polarization decreases until it reaches a fixed value with increasing frequency. This is because the electron exchange Fe^{2+}– Fe^{3+} cannot follow the alternating field above a certain external field frequency. This can be attributed to the prevalence of species such as Fe^{2+} ions, oxygen vacancies, defects at grain boundaries, piles of interfacial dislocations, and voids, among others [30, 28]. The second behavior was observed at relatively high temperatures, where the real part of the dielectric constant initially increased with increasing frequency until reaching a peak, exhibiting conventional relaxation. This behavior can be explained using the Rezlescu assumption [29], where this behavior is attributed to the combined contribution of electrons and holes to the polarization. It is reasonable for the real part of the dielectric constant to decrease as the frequency increases because any species contributing to polarizability is discovered to lag behind the applied field at higher frequencies [31]. Figure 4 illustrates the typical real part of the dielectric behavior of ferrites, which exhibit higher values at low frequencies and decreasing values at higher frequencies. By considering the inhomogeneous dielectric medium explained by Koops' theory with two Maxwell-Wegner-type layers [24, 27], the behavior of the real part of the dielectric constant with frequency is explained [32].

The trend of the dielectric constant έ to reduce with an increase in frequency is natural because any species contributing to polarizability shows lagging behind the applied field at higher frequencies [31]. The normal dielectric behavior of ferrites is shown in Figure 4, where at lower frequencies ε' have higher values and, as frequency increased, decreased. Koops's theory [32] explains this behavior of a dielectric constant with frequency by considering the inhomogeneous dielectric medium explained by Koops's theory with two Maxwell–Wegner type layers [24, 27].

3.4. Dielectric loss factor.

Increases in frequency were accompanied by a reduction in the loss factor. Tan values are influenced by a number of variables, including stoichiometry, Fe^{2+} content, and structural homogeneity, all of which are influenced by sample composition and sintering duration [33]. Figure 5.1 illustrates the variations in loss tangents for synthesized samples as a function of composition. The fact that the charge–carrier hopping frequency stops with the change in polarity after a certain frequency may be the cause of the decline in the loss factor. Hence, Zn^{2+} ions doped in Ba-Ni ferrites lead to a low dielectric loss factor, tan(δ), which can be effectively used in applications requiring high-frequency data storage. For synthesis samples, the loss tangent (tanδ) variables are shown in Figure 5.2. as a function of frequency. Based on Koops' phenomenological mode, the initial drop in tan with an increase in frequency may also be explained [25]. When the frequency of the electron jump between Fe^{2+} and Fe^{3+} is equal to the frequency of the applied field, the peaking nature is observed. An explanation of the resonance peak appearance is provided below. A potential barrier separates the two equilibrium positions, A and B, which have equal potential energies. Ions have the same chance of jumping from B to A as they do from A to B. The natural frequency of the jump between these two states refers to the frequency at which the ion switches positions between these two states. Resonance occurs when an external natural frequency alternating electric field is applied because the

oscillating ions receive the maximum amount of electrical energy while experiencing a significant increase in power loss. As a result, the peaks were as described.

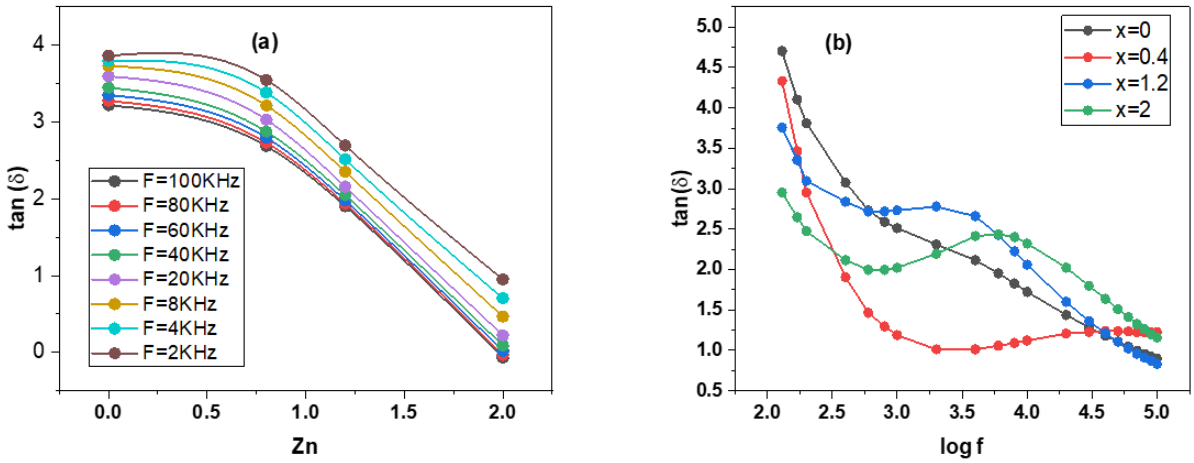

Figure 5.1 (a) Composition dependence of dielectric loss (tanσ) for $BaNi_{2-x}Zn_xFe_{16}O_{27}$ (x=0.0, 0.4, 1.2, and 2). ferrite at different frequencies, (b) Relationship dielectric loss (tanσ) with log frequency at different zinc concentrations at room temperature.

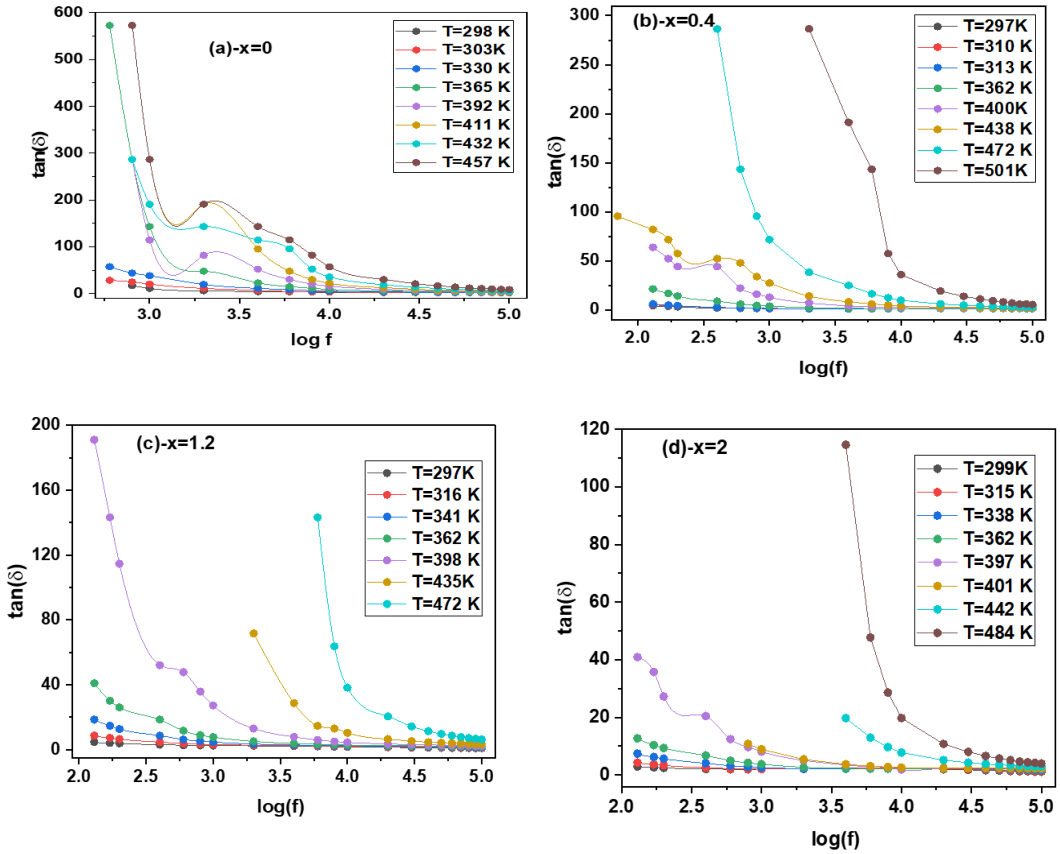

Figure 5.2. Frequency dependence of dielectric loss (tanσ) for $BaNi_{2-x}Zn_xFe_{16}O_{27}$, (a) x= 0.0, (b) x= 0.4,(c) at x = 1.2, and (d) at x = 2, ferrite at different temperatures.

3.5. Electric modulus.

The real (M') and imaginary (M") have been calculated by using the following equations:

$$M' = \frac{\varepsilon'}{\acute{\varepsilon}^2 + \varepsilon''^2} \quad (2)$$

$$M^{"} = \frac{\varepsilon^{"}}{\acute{\varepsilon}^{2} + \varepsilon^{"2}} \quad (3)$$

Equations (2) and (3) represent the real and imaginary parts, respectively, of the electric modulus.

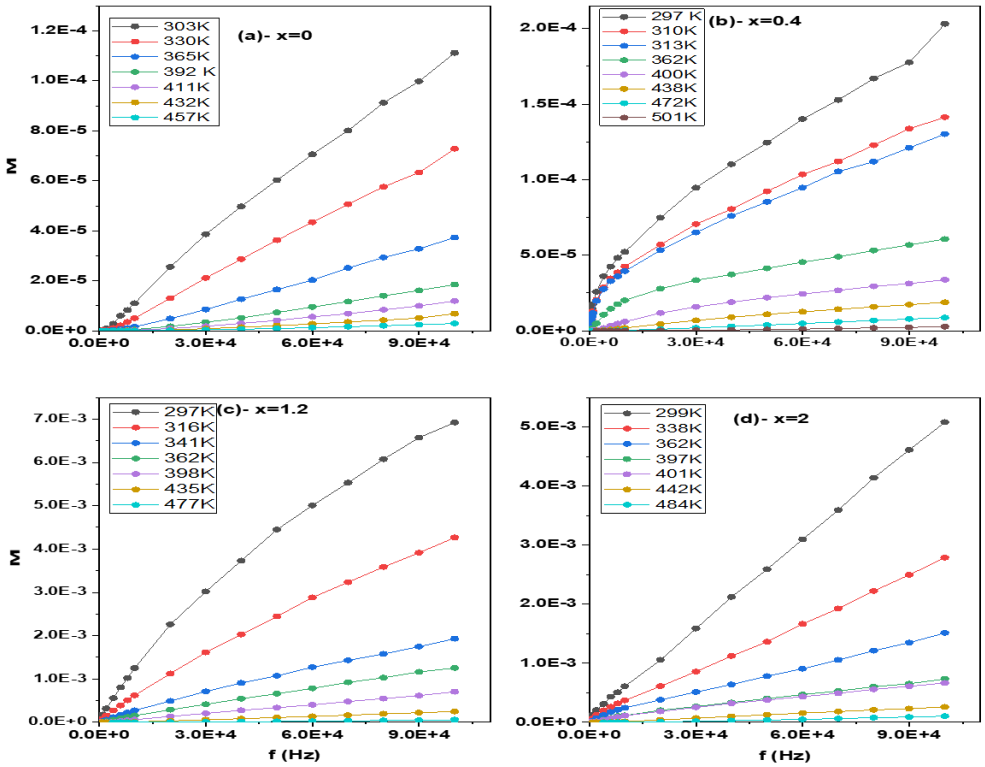

Figure 6. Behavior of real part of electric modulus with frequency for $BaNi_{2-x}Zn_x Fe_{16}O_{27}$, (a) x= 0.0; (b) x= 0.4;(c) at x = 1.2; and (d) at x = 2), at different temperatures.

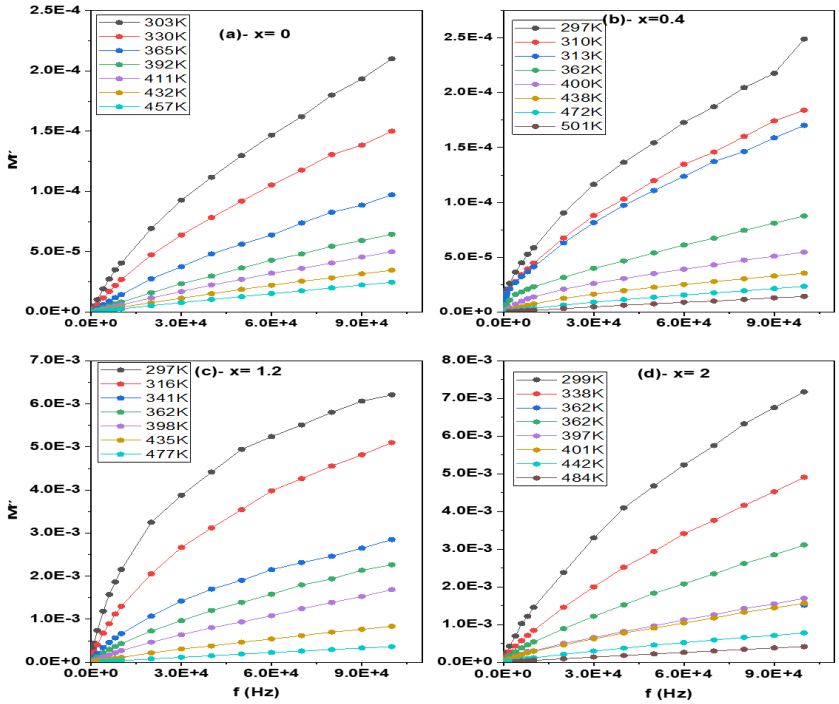

Figure 7. Behavior of imaginary part of electric modulus with frequency for $BaNi_{2-x}Zn_x Fe_{16}O_{27}$, (a) x= 0.0; (b) x= 0.4;(c) at x = 1.2; and (d) at x = 2), at selected temperatures.

The complex dielectric modulus depends on the material's properties, such as the dielectric constant and loss as a function of structure, temperature, and frequency. Because of the electrode polarization (EP) effect, both materials have extremely high dielectric constants and losses at low frequencies. The electric modulus formalism was devised by Macedo et al. to reduce the impact of electrode polarization. Figures 6 and 7, depict frequency's dependence on real M' and imaginary M'' electric modulus at various temperatures of $BaNi_{2-x}Zn_xFe_{16}O_{27}$ ferrites. It is evident that both real M' and imaginary M'' electric modulus increase with frequency up to the maximum value at higher frequencies and also increase with increasing Zn ion concentration, respectively. This behavior is explained by the fact that at high frequencies, the dielectric constant decreases to its minimum value, as shown in Figures S2, and the electric modulus reaches its maximum value.

3.6. Permeability.

The initial magnetic permeability of $BaNi_{2-x}Zn_xF_{16}O_{27}$ at room temperature as a function of composition was calculated using the following relation [34]:

$$\mu_i = \frac{2\pi L}{\mu_\circ N^2 h \ln(\frac{a}{b})} \quad (4)$$

where L is the inductance, N is the number of turns, b is the inner diameter, a is the outer diameter, and h is the height of the core.

Figure 8 shows the variation in the initial permeability with temperature for the series $BaNi_{2-x}Zn_xFe_{16}O_{27}$ (x=0.0, 0.4, 1.2, and 2). As shown in Figure 8. With increasing the zinc concentration, the initial magnetic permeability increased to the maximum value at x = 2. The initial permeability, which is the same as the dielectric constant, is influenced by several factors, including impurity contents, grain structure, compositional, dopant types, crystalline structure, and porosity. The increase in the initial permeability value as Zn concentration increased and vice versa, as shown in Figure 6, is due to the grain growth observed with increasing Zn [21].

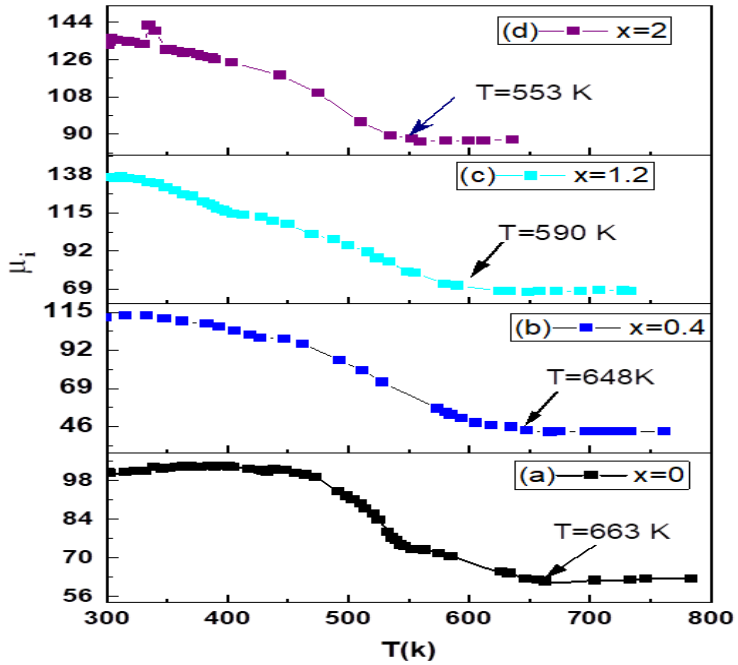

Figure 8. Initial permeability of samples as a function of temperature $BaNi_{2-x}Zn_xFe_{16}O_{27}$ composition: (a) *x*=0, (b) x= 0.4; (d) *x*=1.2, and (c) x= 2.

Additionally, it was found that as zinc content increased, crystallite size and density similarly increased [21] while anisotropy decreased, increasing the initial permeability value [35]. A decrease in initial permeability with temperature is also observed, which is caused by zinc evaporation, which occurs more frequently as the temperature increases. In W-type hexa-ferrites, the magnetic ions are distributed between sub-lattices in parallel alignment that faces away from the c-axis. [36]. Ni^{2+} ions preferentially occupy octahedral sites, Zn^{2+} ions prefer to occupy tetrahedral sites, and Fe^{3+} ions are dispersed over both sites. When the nonmagnetic zinc ions on the tetrahedral sites increase, Fe^{3+} ions travel from tetrahedral to octahedral sites. Because there is less contact between the tetrahedral and octahedral sites due to the reduction in magnetic ions at the tetrahedral site, the Curie temperature decreases, and the initial permeability increases. Because zinc is not magnetic, this behavior occurs naturally, increasing the initial permeability as Zn ions gradually replace Ni ions in the zinc structure.

Accordingly, the behavior of μ(T) for $BaNi_{2-x}Zn_xFe_{16}O_{27}$ (x=0.0, 0.4, 1.2, 2) indicates that the rotation of the dipole momentum in the domain very slowly with temperature and at a certain temperature becomes randomly distributed. At this temperature μ(T) falls to a minimum with a constant value as a function of temperature, which means that the samples transition from phase to phase, from ferrimagnetic materials to paramagnetic materials.

4. Conclusions

It was determined from observations and tests that the replacement of Zn in $BaNi_{2-x}Zn_xFe_{16}O_{27}$ (x=0.0, 0.4, 1.2, 2) significantly modifies modifications to the electrical and magnetic properties of nanoferrites. The dispersion behavior of a normal dielectric was ascertained can be referred to as the Maxwell–Wagner kind of polarization. The dielectric results showed that the zinc concentration at composition x = 0.4 was sufficient to reduce the dielectric constant and loss tangent at low frequencies, while the dielectric constant had much better results and showed maximum values at x = 0.4. Such material can be dangerously utilized in perpendicular magnetic recording media. However, the dielectric properties of this sample make it a suitable candidate for flexible supercapacitors. Based on Koop's phenomenological mode, the initial loss tangent drop of tan with an increase in frequency may also be explained. Increasingly shifted shoulders also guarantee the presence of two different types of charge carriers in (έ) with increasing temperature curves towards higher frequencies. The dielectric results demonstrate that a Zn dopant concentration beyond Zn = 0.4 was adequate to reduce both loss tangent and dielectric constant at low frequencies. This study reveals a wide range of variations in Zn^{2+} ion concentration as well as frequency variation, which have not been reported previously. Generally, the decrease in dielectric parameters such as loss tangent and dielectric constant resulting from incorporating Zn^{+2} ions advocate the appropriation of these materials in high-frequency applications such as recording media, sensors, circulators, microwave devices, electronic devices, and phase shifters. As Zn^{2+} ion replacement increases, the initial magnetic permeability increases. This could be explained by magnetic Ni^{2+} ions substituting for nonmagnetic Zn^{2+} ions. Substituting Zn ions enhances the dielectric constant, dielectric loss, magnetic loss, and permeability.

Funding

This research received no external funding.

Acknowledgments

The authors would like to thank Dr. A.M. Abo El Ata and the Physics Department, Faculty of Science, Tanta University, Tanta, Egypt, for his help during the experimental measurements for the present work.

Conflicts of Interest

The authors declare no conflict of interest.

References

1. Nanoparticle Technology Handbook; Hosokawa, M., Ed.; 1st ed.; Elsevier: Amsterdam, Netherlands ; Boston [Mass.], **2007**, https://shop.elsevier.com/books/T/A/9780444531223.
2. Patel, J.K.; Patel, A.; Bhatia, D. Introduction to Nanomaterials and Nanotechnology. In Emerging Technologies for Nanoparticle Manufacturing; Patel, J.K., Pathak, Y.V., Eds.; Springer International Publishing: Cham, **2021**; pp. 3–23, https://link.springer.com/chapter/10.1007/978-3-030-50703-9_1.
3. Dippong, T.; Levei, E.A.; Cadar, O. Recent Advances in Synthesis and Applications of MFe2O4 (M = Co, Cu, Mn, Ni, Zn) Nanoparticles. *Nanomaterials* **2021**, *11*, 1560, https://doi.org/10.3390/nano11061560.
4. Kaur, M.; Kim, T.; Kim, W.S. New Frontiers in 3D Structural Sensing Robots. Adv. Mater. **2021**, *33*, 2002534, https://doi.org/10.1002/adma.202002534.
5. Dhiman, P.; Rana, G.; Goyal, D.; Goyal, A. Basics of Ferrites: Types and Structures. In Ferrites and Multiferroics: Fundamentals to Applications; Bhargava, G.K., Bhardwaj, S., Singh, M., Batoo, K.M., Eds.; Springer: Singapore, **2021**; pp. 1–25, https://link.springer.com/chapter/10.1007/978-981-16-7454-9_1.
6. Vinnik, D.A.; Gudkova, S.A.; Zhivulin, V.E.; Trofimov, E.A. Ferrite-Based Solid Solutions: Structure Types, Preparation, Properties, and Potential Applications. *Inorg Mater* **2021**, *57*, 1109–1118, https://doi.org/10.1134/S0020168521110133.
7. Coey, J.M.D. Magnetic Oxides and Other Compounds. In Handbook of Magnetism and Magnetic Materials; Coey, J.M.D., Parkin, S.S.P., Eds.; Springer International Publishing: Cham, **2021**; pp. 847–922, https://link.springer.com/referenceworkentry/10.1007/978-3-030-63210-6_17.
8. Arthur Charles Prabakar; Govindarasu Killivalavan; Dhananjayan Sivakumar; K. Chandra Babu Naidu; Balaraman Sathyaseelan; Krishnamoorthy Senthilnathan; Iruson Baskaran; Elayaperumal Manikandan; M. Balaraju. Exploring Structural, Morphological, and Magnetic Properties of Zinc Nickel Ferrites Systems Nanocomposites. *Biointerface Res Appl Chem* **2020**, *11*, 7785–7793, https://biointerfaceresearch.com/wp-content/uploads/2020/07/20695837111.77857793.pdf.
9. Vinnik, D.A.; Zhivulin, V.E.; Starikov, A.Yu.; Gudkova, S.A.; Trofimov, E.A.; Trukhanov, A.V.; Trukhanov, S.V.; Turchenko, V.A.; Matveev, V.V.; Lahderanta, E.; et al. Influence of Titanium Substitution on Structure, Magnetic and Electric Properties of Barium Hexaferrites BaFe12−xTixO19. *Journal of Magnetism and Magnetic Materials* **2020**, *498*, 166117, https://doi.org/10.1016/j.jmmm.2019.166117.
10. Mitrović, N.S.; Nedeljković, B.; Obradović, N. Magnetic Features of MnZn Ferrite for Electronic Applications. Program and the Book of abstracts / Serbian Ceramic Society Conference Advanced Ceramics and Application IX : New Frontiers in Multifunctional Material Science and Processing, Serbia, Belgrade, 20-21. September **2021** 2021, 59–59, https://dais.sanu.ac.rs/handle/123456789/11901?locale-attribute=en.
11. Khan, S.B.; Irfan, S.; Lee, S.-L. Influence of Zn+2 Doping on Ni-Based Nanoferrites; (Ni1−x ZnxFe2O4). Nanomaterials **2019**, *9*, 1024, https://doi.org/10.3390/nano9071024.
12. Pradhan, A.K. Effect of Mo Substitution on Structural, Dielectric, Electrical and Magnetic Properties of Cobalt-Zinc Spinel Ferrites. Thesis, Vidyasagar University, Midnapore, West Bengal, India, **2021**, http://inet.vidyasagar.ac.in:8080/jspui/handle/123456789/6012.
13. Kumar, A.M.; Rao, K.S.; Varma, M.C.; Rao, K.H. Investigations of Surface Spin Canting in Ni-Zn Nanoferrite and Its Development as Magnetic Core for Microwave Applications. *Journal of Magnetism and Magnetic Materials* **2019**, *471*, 262–266, https://doi.org/10.1016/j.jmmm.2018.09.060.
14. Thakur, P.; Taneja, S.; Chahar, D.; Ravelo, B.; Thakur, A. Recent Advances on Synthesis, Characterization and High Frequency Applications of Ni-Zn Ferrite Nanoparticles. *Journal of Magnetism and Magnetic Materials* **2021**, *530*, 167925, https://doi.org/10.1016/j.jmmm.2021.167925.
15. Khan, S.B.; Irfan, S.; Lee, S.-L. Influence of Zn+2 Doping on Ni-Based Nanoferrites; (Ni1−x ZnxFe2O4). *Nanomaterials* **2019**, *9*, 1024, https://doi.org/10.3390/nano9071024.
16. Pošković, E.; Franchini, F.; Ferraris, L.; Carosio, F.; Actis Grande, M. Rapid Characterization Method for SMC Materials for a Preliminary Selection. *Applied Sciences* **2021**, *11*, 12133, https://doi.org/10.3390/app112412133.
17. Ahmed, M.A.; Okasha, N.; El-Dek, S.I. Preparation and Characterization of Nanometric Mn Ferrite via Different Methods. *Nanotechnology* **2008**, *19*, 065603, https://doi.org/10.1088/0957-4484/19/6/065603.

18. Andalib, P.; Harris, V.G. Grain Boundary Engineering of Power Inductor Cores for MHz Applications. *Journal of Alloys and Compounds* **2020**, *832*, 153131, https://doi.org/10.1016/j.jallcom.2019.153131.
19. Gegevičius, R.; Franckevičius, M.; Gulbinas, V. The Role of Grain Boundaries in Charge Carrier Dynamics in Polycrystalline Metal Halide Perovskites. *Eur. J. Inorg. Chem.* **2021**, *2021*, 3519–3527, https://doi.org/10.1002/ejic.202100360.
20. Li, W.; Fa-Shen, L. *Structural and Magnetic Properties of Co 1- x Zn x Fe 2 O 4 Nanoparticles. Chinese Phys. B* **2008**, *17*, 1858–1862, https://doi.org/10.1088/1674-1056/17/5/052.
21. AL-Hammadi , A.H.; Khoreem , Sadiq H. Investigations on Optical and Electrical Conductivity of Ba/Ni/Zn/Fe16O27 Ferrite Nanoparticles. *Biointerface Res Appl Chem* **2022**, *13*, 168, https://doi.org/10.33263/BRIAC132.168.
22. Khoreem , Sadiq H. AL-Hammadi , A.H.; Synthesis and Unveiling the Effect of Nonmagnetic Zn2+ Ions on Enrichment of Structural Properties of BariumNickel Ferrites**.** *Biointerface Res Appl Chem* **2023**, *13*,488,https://doi.org/10.33263/BRIAC135.488.
23. Janu, Y.; Chaudhary, D.; Singhal, N.; Chauhan, V.S.; Balwa, C.L.; Saini, L.; Patra, M.K. Tuning of Electromagnetic Properties in Ba(MnZn)XCo2(1-x)Fe16O27/NBR Flexible Composites for Wide Band Microwave Absorption in 6–18 GHz. *Journal of Magnetism and Magnetic Materials* **2021**, *527*, 167666, https://doi.org/10.1016/j.jmmm.2020.167666.
24. Henaish, A.M.A.; Ali, M.M.; Refaay, D.E.E.; Weinstein, I.A.; Hemeda, O.M. Synthesis, Electric and Magnetic Characterization of Nickel Ferrite/PANI Nano-Composite Prepared by Flash Auto Combustion Method. *J Inorg Organomet Polym* **2021**, *31*, 731–740, https://doi.org/10.1007/s10904-020-01737-w.
25. AL-Hammadi , A.H.; Khoreem , Sadiq H. Influence of Zn^{+2} Doping on Dielectric Properties of BaBased Nanoferrites. Biointerface Res Appl Chem **2022**, *13*, 256, https://doi.org/10.33263/BRIAC133.256.
26. Jebli, M.; Rayssi, Ch.; bouzidi, S.; Dhahri, J.; Ben Henda, M.; Zaidi, N. Effect of Nb Substitution on the Structural, Dielectric and Modulus Character of Ba0.97La0.02TiO3 Ceramics. *Inorganic Chemistry Communications* **2021**, *129*, 108628, https://doi.org/10.1016/j.inoche.2021.108628.
27. Nguyen, B.H.; Zhuang, X.; Rabczuk, T. Numerical Model for the Characterization of Maxwell-Wagner Relaxation in Piezoelectric and Flexoelectric Composite Material. *Computers & Structures* **2018**, *208*, 75–91, https://doi.org/10.1016/j.compstruc.2018.05.006.
28. Mujasam Batoo, K. Study of Dielectric and Impedance Properties of Mn Ferrites. *Physica B: Condensed Matter* **2011**, *406*, 382–387, https://doi.org/10.1016/j.physb.2010.10.075.
29. Akhter, S.; Paul, D.P.; Hakim, M.A.; Saha, D.K.; Das, H.N.; Parveen, A.; Anjuman, B. Transport Properties of Polycrystalline Mixed Copper-Zinc Ferrites. *Mat. Res.* **2018**, *21*, https://doi.org/10.1590/1980-5373-MR-2017-0655.
30. Chhantbar, M.C.; Modi, K.B.; Joshi, H.H. Compositional, Temperature and Frequency Dependence of Dielectric Behaviour of Zinc Substituted Copper- Ferri-Chromates. *J Mater Sci* **2007**, *42*, 6989–6995, https://doi.org/10.1007/s10853-006-1240-z
31. AL-Hammadi , A.H. Khoreem , Sadiq H.. Impact of Zinc Substitution on AC Conductivity Behaviors of Hexagonal Ba-Ni Ferrite Nanoparticle. *Biointerface Res Appl Chem* **2023**, *13*, 364, https://doi.org/10.33263/BRIAC134.364.
32. Hajlaoui, M.E.; Gharbi, S.; Dhahri, E.; Khirouni, K. Impedance Spectroscopy and Giant Permittivity Study of ZnFe2O4 Spinel Ferrite as a Function of Frequency and Temperature. *Journal of Alloys and Compounds* **2022**, *906*, 164361, https://doi.org/10.1016/j.jallcom.2022.164361.
33. Rehman, A. ur; Shaukat, S.F.; Haidyrah, A.S.; Akhtar, M.N.; Ahmad, M. Synthesis and Investigations of Structural, Magnetic and Dielectric Properties of Cr-Substituted W-Type Hexaferrites for High Frequency Applications. *J Electroceram* **2021**, *46*, 93–106, https://doi.org/10.1007/s10832-021-00246-7.
34. Ghodake, J.S.; Shinde, T.J.; Patil, R.P.; Patil, S.B.; Suryavanshi, S.S. Initial Permeability of Zn–Ni–Co Ferrite. *Journal of Magnetism and Magnetic Materials* **2015**, *378*, 436–439, https://doi.org/10.1016/j.jmmm.2014.11.041.
35. R.V. Mangalaraja et al. Effect of composition on initial permeability of Ni1-*x*Zn*x*Fe2O4 prepared by flash combustion technique. *Materials Science and Engineering A* **2008**, *476*, 234–239, https://doi.org/10.1016/j.msea.2007.05.078.
36. You, J.-H.; Yoo, S.-I. Improved Magnetic Properties of Zn-Substituted Strontium W-Type Hexaferrites. *Journal of Alloys and Compounds* **2018**, *763*, 459–465, https://doi.org/10.1016/j.jallcom.2018.05.296.